Investigating the determinants of mammalian Mastl kinase activation

Mehmet Erguven[1,2], M. Kasim Diril[1,2,3*]

[1]Izmir Biomedicine and Genome Center, Mithatpasa Ave., 35340, Izmir, Turkey

[2]Izmir International Biomedicine and Genome Institute, Dokuz Eylul University, 35340, Izmir, Turkey

[3]Department of Medical Biology, School of Medicine, Dokuz Eylul University, Izmir, Turkey

***Corresponding Author:**

E-mail: kasim.diril@ibg.edu.tr

KEYWORDS

Mastl, kinase activation, phosphorylation, cell cycle

ABSTRACT

Mastl (Greatwall) kinase is an essential mitotic protein kinase. Mastl is an atypical member of AGC family with a unique long stretch of non-conserved middle region. The mechanism of its phosphorylation dependent activation has been studied in Xenopus egg extracts, revealing several phosphosites that were suggested to be crucial for kinase activation. These residues correspond to T193 and T206 in the activation loop, and S861 in the C-tail of mouse Mastl. By combining a chemically inducible knockout system to deplete the endogenous Mastl and a viral expression system to ectopically express the mutant variants, we obtained a viable knockout clone that expresses the S861A and S861D mutants. We observed that proliferation rates of the $Mastl^{S861A}$ and $Mastl^{S861D}$ clones were comparable. Our results have revealed that phosphorylation of the turn motif phosphosite (S861) is auxiliary and it is not indispensable for Mastl function.

1. INTRODUCTION

1.1. Function of Mastl in mitosis

Mitosis is the phase of cell cycle in which the genetic material of the parental cell is equally distributed to the daughter cells. The phase is characterized by the dramatic and rapid alterations in the biochemical and the morphological state of the cell (Alberts, 2015; Glover, 2012). Initiation, progression, and termination of mitosis has to be strictly regulated by multiple layers of regulation mechanisms. These are post-translational modification, subcellular localization, and proteolytic degradation (Baxter et al., 2008). Post-translational regulation by phosphorylation is the major regulator of mitosis. Therefore, the initiation of the phase is governed by mitotic protein kinases (H. Kim et al., 2016). Cdk1/cyclin B is the primary kinase that governs mitosis (M. K. Diril et al., 2012; Santamaría et al., 2007). Key mitotic kinases work in a network, layered of positive feedback loops that construct a robust signaling cascade. This signaling cascade quickly activates the mitotic substrates. Mitosis is terminated at the beginning of the anaphase. During termination of the phase, the mitotic signals are quenched by antagonistic protein phosphatases and the ubiquitin ligases. Actions of these antagonistic factors ultimately revert the cellular changes that occurred during mitosis. The balance between the mitotic factors and the anti-mitotic factors is set on a cell cycle checkpoint named Spindle assembly checkpoint (SAC). In general, while mitotic factors maintain SAC signaling, anti-mitotic factors suppress SAC in order to allow the cell to proceed to anaphase. Under normal circumstances, transition from metaphase to anaphase is blocked until all the kinetochores are correctly bound bilaterally (Ciliberto & Shah, 2009). SAC signaling preserves the genomic stability by delaying anaphase until each kinetochore-microtubule attachment is correct.

At the top of the mitotic signaling cascade, active Cdk1/cyclin B complex takes place. The active Cdk1 activates its activator Cdc25 (Yu et al., 2006) and inhibits its inhibitors Wee1 and Myt1 kinases. This positive feedback loop allows rapid accumulation of the active Cdk1 pool. Cdk1 activates its mitotic substrates and its downstream protein kinases activate their mitotic substrates, initiating a signaling cascade. Most of these phosphorylations on downstream proteins result in activation of factors that promote mitosis and inhibition of factors that promote mitotic exit. To be able to preserve the mitotic state of the cell, mitotic phosphorylations have to be maintained throughout the phase. Therefore, a strong autoamplification loop has to be

coupled with inhibition of the factors that promote mitotic exit (Gharbi-Ayachi et al., 2010). PP2A (protein phosphatase 2A) is the primary antagonist of Cdk1 during mitosis. This phosphatase is indirectly inhibited by Mastl (Microtubule-associated serine/threonine kinase like). Mastl is the human orthologue of Gwl (Greatwall) kinase, first identified in Drosophila. Mastl kinase phosphorylates two highly homologous, small, thermostable proteins named Arpp19 and Ensa at their Serine 62 and Serine 67 residues, respectively. These two phosphoproteins specifically bind and inhibit B55∂ bound PP2A. Inhibition of PP2A-B55∂ results in the rapid accumulation of phosphorylations on mitotic substrates. This inhibition also prevents the removal of inhibitory phosphorylations on Wee1 and Myt1, and activating phosphorylation of Cdc25, further supporting the autoamplification loop and the activity of MPF (maturation promoting factor) (M.-Y. Kim et al., 2012; Kishimoto, 2015; S. Mochida et al., 2010; Satoru Mochida & Hunt, 2012; Slupe et al., 2011).

Due to its crucial function in mitosis, Mastl kinase is an essential mitotic protein kinase. Loss-of-function studies have shown that in the absence of Mastl, SAC signaling is weakened (Diril et al., 2016). The weakened SAC signaling cannot further delay anaphase. The cell does not have the opportunity to correct every aberrant kinetochore attachment. Consequently, abnormal chromosomal segregation and anaphase bridges occur. The anaphase bridges prevent closure of the cleavage furrow. In other words, mitosis cannot be completed (Alvarez-Fernandez et al., 2013).

1.2. Catalytic elements of protein kinases

Protein kinases are transferase class of enzymes that transfer the gamma phosphate of ATP to the hydroxyl group of serine, threonine, tyrosine, or histidine residues of the substrate protein. Protein kinases are bilobal enzymes and the active site is buried in a cleft between its two lobes. Several catalytically crucial segments or residues located within the catalytic cleft are the activation loop, DFG motif (within the activation loop), catalytic aspartate (within the DFG motif), glycine-rich loop, and conserved lysine.

The common kinase fold is constituted of a β-sheet-rich smaller N-lobe and an α-helix-rich larger C-lobe, connected through a loop segment. This loop encompasses the activation loop, which incompasses the DFG motif. At the N-terminal proximity of this connecting loop, DFG motif takes place. The catalytic aspartate is located in the

DFG (Asp-Phe-Gly) motif. Two divalent cations are accommodated into the ATP binding pocket in order to stabilize the negatively charged phosphate groups of the ATP. The phosphate groups of ATP and the catalytic aspartate side chain together chelate these divalent cation cofactors, which are usually magnesium and also can be manganese (Diamant et al., 1995). The catalytic aspartate is responsible for the transfer of the ATP γ-phosphate to the target residue of the substrate protein or peptide. The glycine-rich loop backbone, chelated cofactors, and a conserved lysine coordinate the ATP through charged or polar interactions with its α- and β-phosphates. The purine moiety contributes to the coordination process by establishing specific hydrogen bonds with the hinge region backbone (Endicott et al., 2012) (Figure 1).

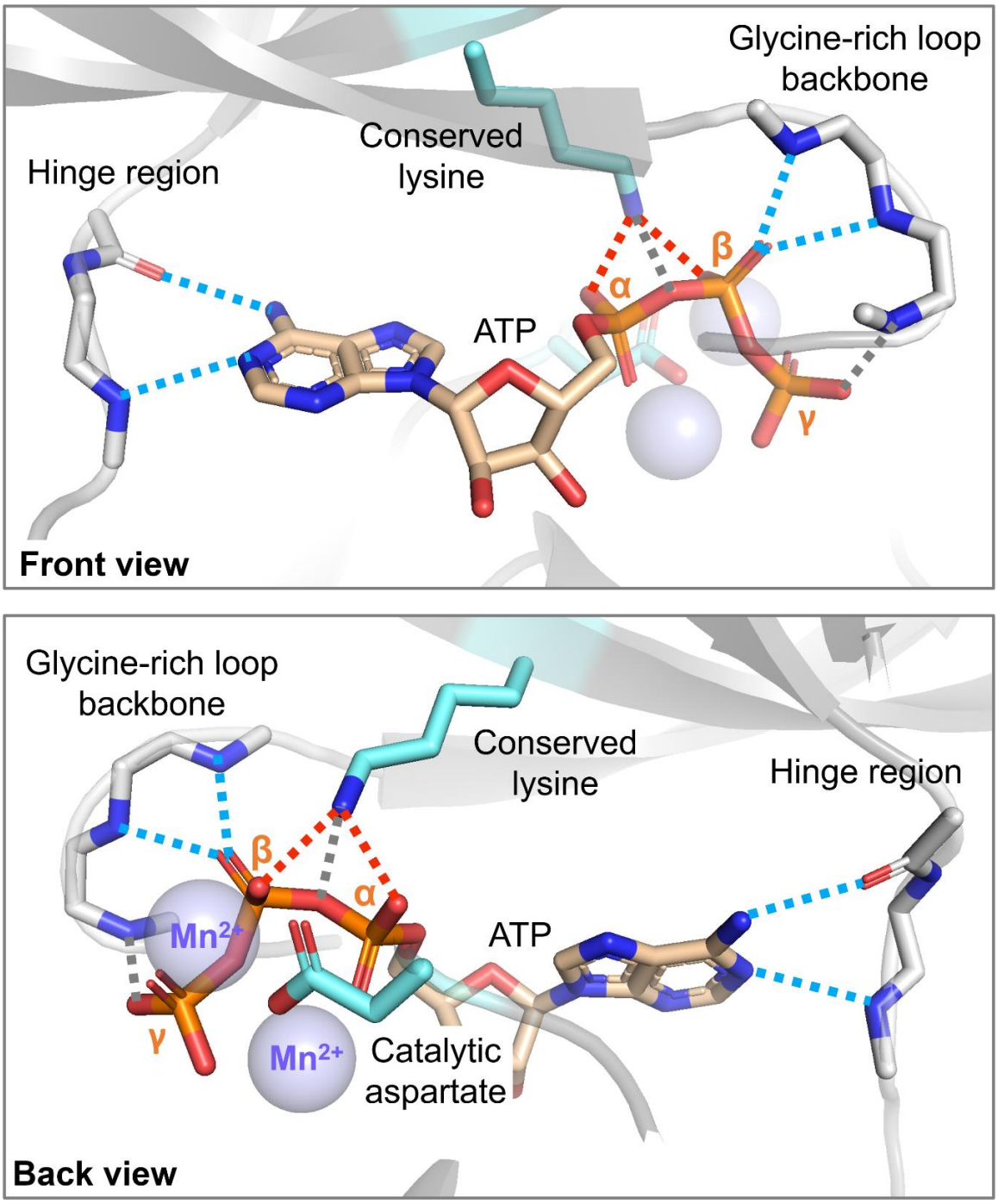

Figure 1. The crystal structure of the catalytic subunit of ATP-bound c-AMP-dependent protein kinase (PDB entry 1ATP) (Zheng et al., 1993). The hinge region and glycine-rich loop backbones, catalytic aspartate, conserved lysine and ATP are shown in stick forms. The blue, orange, and red colored atoms are nitrogen, phosphorus, and oxygen, respectively. The observable ion-ion (salt bridge), ion-dipole (H-bond), and dipole-dipole (H-bond) interactions between the enzyme and the ATP are depicted as red, gray, and blue colored dashed lines, respectively. Manganese ions are depicted as transparent spheres.

Activation loop starts with the DFG motif and typically encompasses the following 20-30 residues of the connecting loop (Modi & Dunbrack, 2019). This segment functions as a docking site for the substrate peptide. The sequence of the activation loop confers substrate specificity by determining the target consensus sequence through specific interactions. The conformation of the activation loop determines whether the enzyme is inactive or active by affecting three factors. These are accession of ATP to the ATP binding pocket, accession of the peptide substrate to the peptide binding groove, and orientation of the catalytic aspartate side chain. The inactive and active conformations of activation loop are defined as DFG-in and DFG-out conformations, respectively (Figure 2). Under physiological conditions, the transition between DFG-in and DFG-out conformation is determined by the phosphorylation status of the activation loop. According to the general kinase activation model, DFG-in conformation is induced by activation loop phosphorylation. The phosphorylation event can be executed by upstream protein kinases or it can be autophosphorylation (Adams, 2003; Vijayan et al., 2015). In its inactive state, the activation loop simultaneously blocks its peptide substrate docking site and the ATP binding pocket. The catalytic aspartate side chain is tilted away from the ATP binding pocket. In its active state, activation loop simultaneously exposes its peptide substrate docking site and releases the ATP binding pocket. The catalytic aspartate side chain is tilted inwards the ATP binding pocket (Figure 2) (Huse & Kuriyan, 2002).

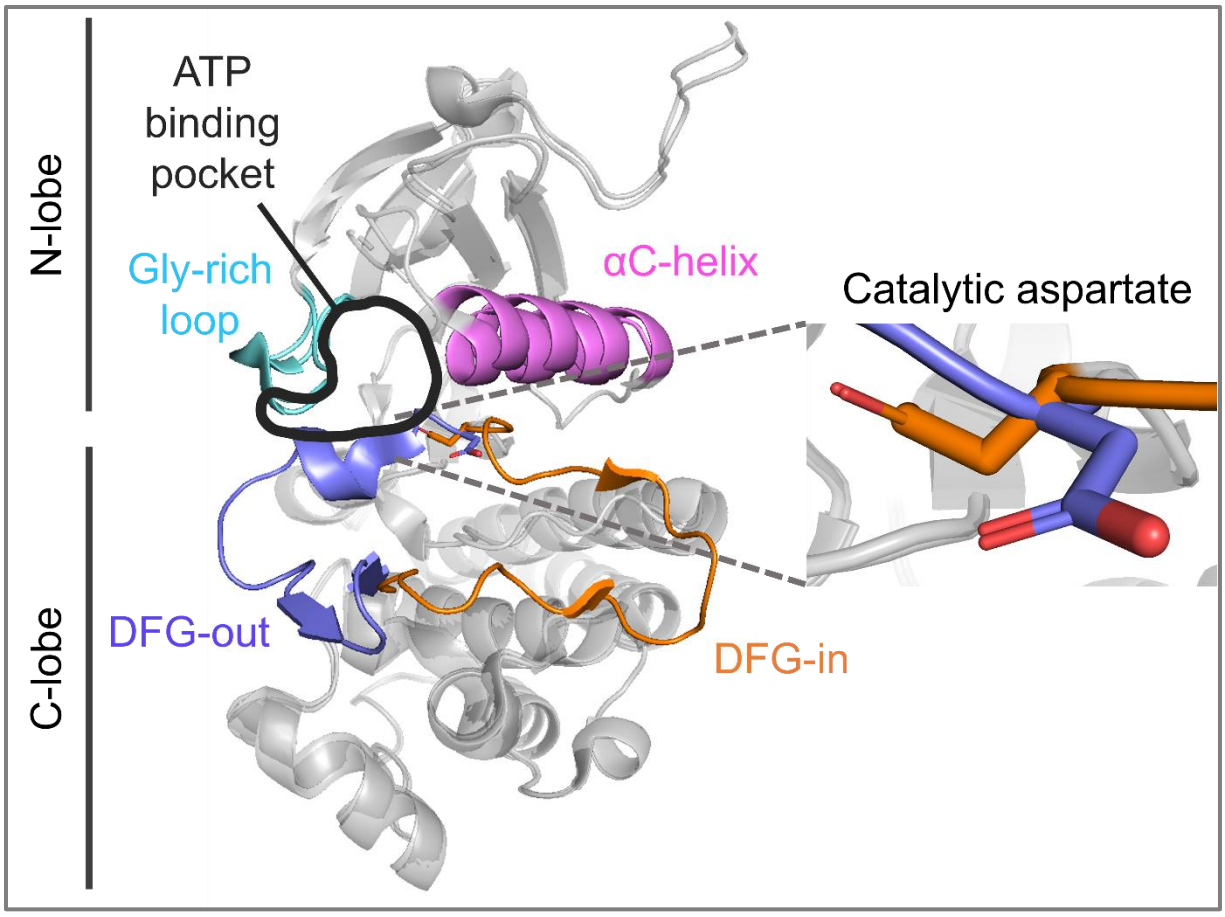

Figure 2. The structural organization of protein kinases. The catalytically important segments glycine-rich loop (cyan), activation loop, and αC-helix (pink) are represented. DFG-in and DFG-out conformations of Abl kinase were superposed (PDB entries 3KF4 and 3KFA, respectively) (Zhou et al., 2010). In the DFG-in conformation (orange), activation loop exposes the ATP binding pocket while orienting the catalytic aspartate towards the ATP binding pocket. In the DFG-out conformation (purplish blue), activation loop occludes the ATP binding pocket and orients the catalytic aspartate away from the ATP binding pocket.

In AGC family of protein kinases, phosphorylation of the activation loop can only partially activate the enzyme. A unique feature of AGC kinases is that the core catalytic elements needs to be stabilized through long-distance intramolecular interactions, in an allosteric manner. These interacting partners are C-tail from C-lobe and αC-helix from N-lobe. The C-tail has two important regions that directly interact with the N-lobe. These are the turn motif and the HF motif (hydrophobic motif, FXXF). NLT (N-lobe tether) encompasses the stretch that proceeds the turn motif towards its C-terminal and the HF motif. The C-tail is regulated by both cis- and trans-phosphorylation. The

conserved serine/threonine in the turn motif is phosphorylated. By the help of this phosphosite, the C-tail is docked to the basic cavity at the N-lobe. Extending from this initial docking point via NLT, the HF motif reaches the hydrophobic pocket at the N-lobe. The HF motif enhances the hydrophobic packing by inserting the benzyl groups of its conserved phenylalanines into this hydrophobic pocket. As a result, HF motif of the C-tail, αC-helix of the N-lobe, and the proximal β-strand of the N-lobe antiparallel β-sheet together construct a hydrophobic groove. This packing allows the C-tail to reposition the αC-helix. Ultimately, the conserved glutamate located in the αC-helix and the conserved lysine located in the ATP binding pocket form a salt bridge. As explained previously, this conserved lysine functions in coordination of the ATP. Given this vital function of the lysine in the enzyme activity, it is clear that the C-tail indirectly aids the active site for coordination of the ATP. Briefly, through an intramolecular allosteric regulation, a conformational domino effect occurs. HF motif repositions the αC-helix, αC-helix coordinates the conserved lysine, and then this lysine ultimately contributes to coordination of the ATP (Figure 3). Using the crystal structure of human PKC-ι (PDB entry 3A8W) (Takimura et al., 2010), the complete molecular machinery is visualized in Figure S1.

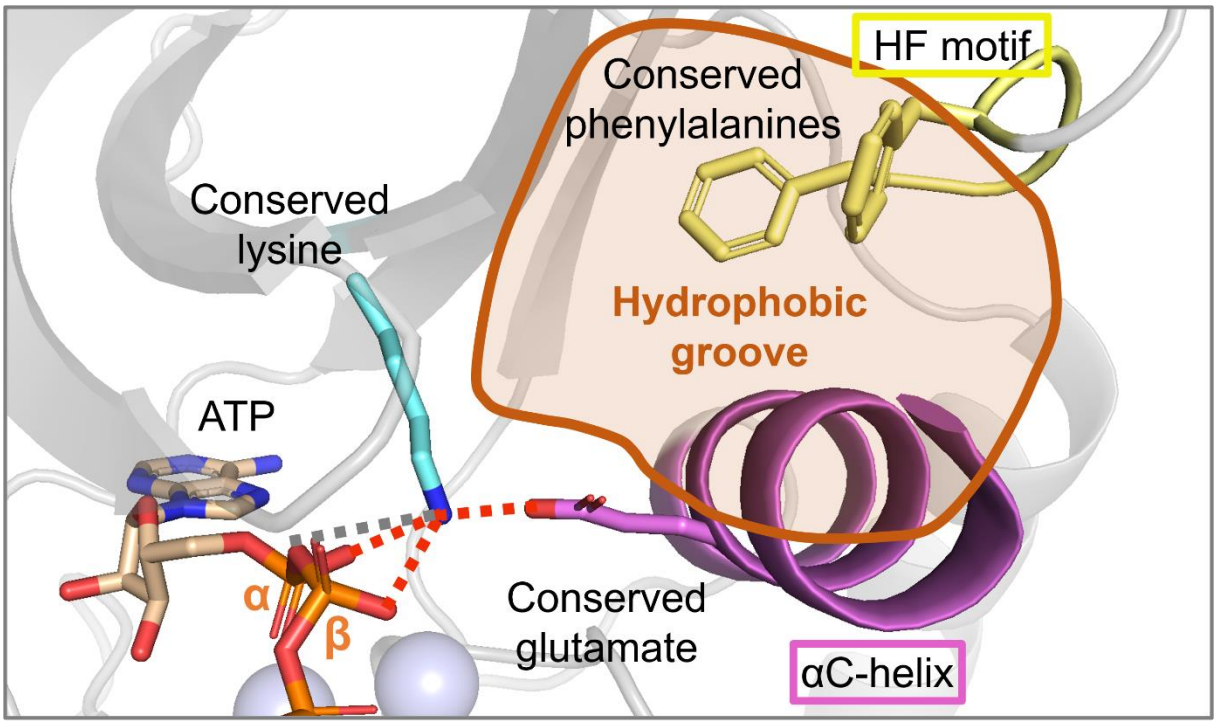

Figure 3. The crystal structure of the catalytic subunit of ATP-bound c-AMP-dependent protein kinase (PDB entry 3X2W) (Das et al., 2015). The conserved lysine and glutamate, and the conserved phenylalanine residues of the HF motif are shown in

stick forms. The blue, orange, and red colored atoms are nitrogen, phosphorus, and oxygen, respectively. The observable ion-ion (salt bridge), ion-dipole (H-bond), and dipole-dipole (H-bond) interactions between the enzyme and the ATP are depicted as red, gray, and blue colored dashed lines, respectively. Magnesium ions are depicted as transparent spheres. The hydrophobic groove is indicated by the transparent brown area. The αC-helix (violet), HF motif (yellow), and the proximal β-strand (transparent gray) together form the hydrophobic groove.

Other routes through which C-tail exerts its regulatory effects are the other intramolecular interactions that it establishes. The C-tail extends over the N-lobe to find the docking sites for the phosphorylated turn motif and HF motif. Doing so, the remaining N-terminal segment of the C-tail is vertically wrapped around the kinase. This wrapped middle C-tail stretch engages in other intramolecular interactions. Other more general C-tail interacting partner is the linker domain (Kannan et al., 2007; Pearce et al., 2010; Taylor et al., 2012).

1.3. Activation of Mastl kinase

Mastl (Microtubule-associated serine/threonine kinase like) is a unique serine/threonine protein kinase among the AGC family kinases. It has an unusually long (~500 residues) linker region between its N-terminal and C-terminal lobes. Studies on Xenopus egg extracts have revealed three phosphosites that are critical for the activation of Mastl (Blake-Hodek et al., 2012). Positions of these residues in mouse Mastl are respectively T193, T206, and S861. T193 and T206 are located in the activation loop within Cdk1 consensus motifs (proline-directed) and are phosphorylated by Cdk1 *in vitro*. These two phosphosites are necessary for nuclear export of Mastl before NEBD (nuclear envelope breakdown) (Alvarez-Fernandez et al., 2013).

According to the currently accepted model, phosphorylation by Cdk1 partially activates Mastl. This activation loop phosphorylation corresponds to the initial step of general kinase activation. The activation loop shifts from DFG-out conformation to DFG-in conformation. Upon this partial activation, Mastl undergoes cis-autophosphorylation by phosphorylating its turn motif phosphosite S861 (Blake-Hodek et al., 2012). As explained in the previous section, in AGC kinases, this turn motif phosphoresidue is docked to a basic patch on the N-lobe, contributing to the tethering

of the C-tail over N-lobe. In this regard, S861 turn motif phosphorylation serves as a means to guide the HF motif towards the αC-helix. However, in case of Mastl, the C-tail of the enzyme is short, it does not possess a known HF motif, therefore it cannot reach the hydrophobic pocket (Figure 4). Mastl compensates for this shortfall of structural regulation by utilizing the HF motif of other AGC kinases (Vigneron et al., 2011).

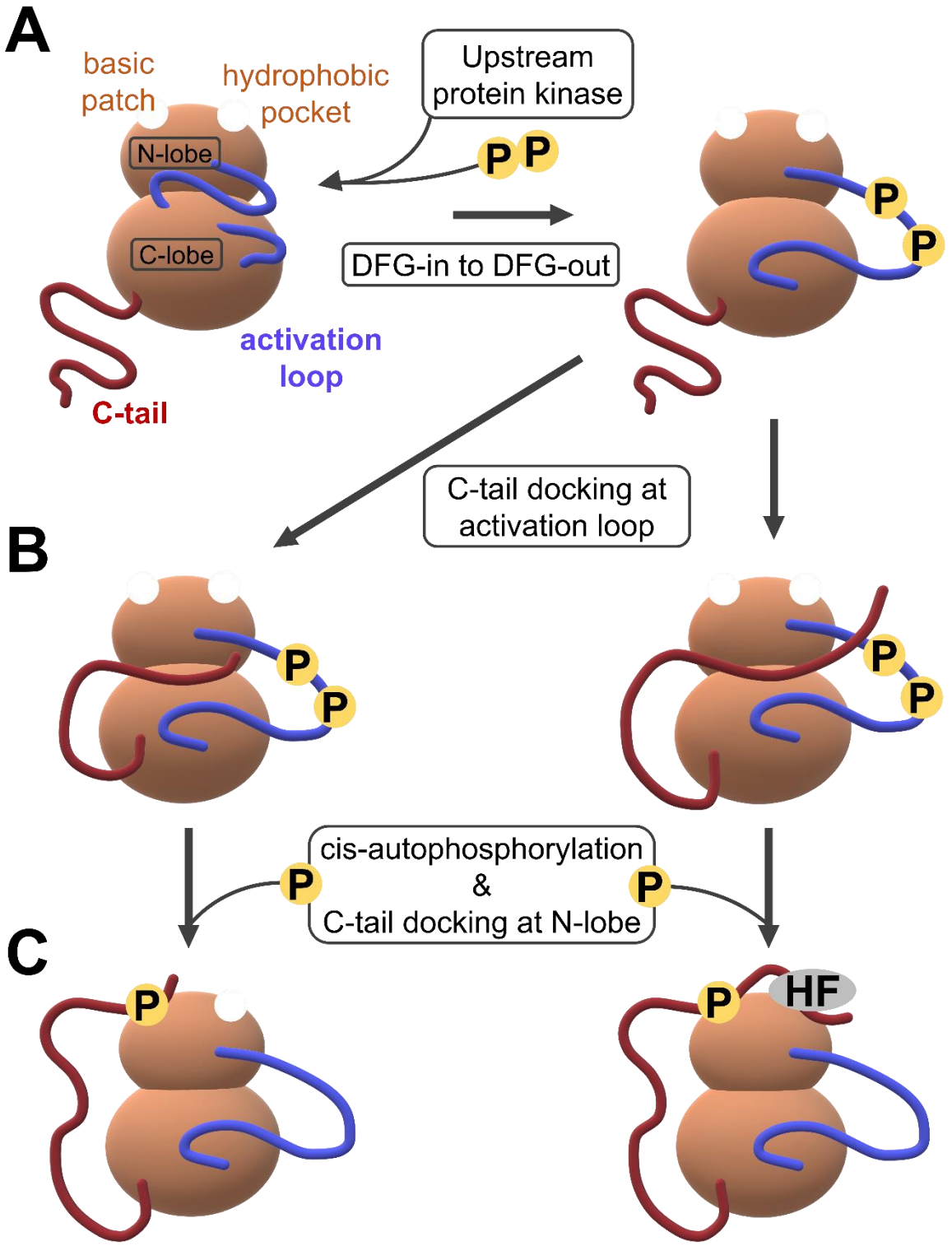

Figure 4. Comparison of the general AGC kinase activation model and the accepted activation mechanism of Mastl kinase. The bilobal protein kinase structure is depicted as light-brown bubbles. The white indents at the top-left and top-right positions of the N-lobe indicate the basic patch and the hydrophobic pocket, respectively. The activation loop and the C-tail are depicted as blue and dark-red lines, respectively. (A)

In general, protein kinases are activated by phosphorylation of their activation loops. The cartoon models given in the figures (B) and (C) show the difference between the activation of Mastl (left) and Mastl with an imaginary normal C-tail (right) that possess an HF motif. For simplicity, the extended NCMR domain is not represented in the illustrated Mastl kinase structures.

The phosphorylation-dependent activation mechanism of Mastl and the biological significance of its NCMR had been extensively studied in Xenopus oocyte extracts and *in vitro* (Blake-Hodek et al., 2012; Vigneron et al., 2011). According to the currently accepted model, phosphorylation of two activation loop phosphosites (T193 and T206 in mouse) and the turn motif phosphosite (S861 in mouse) has been proven to be crucial for the activation of Mastl. In the present study, we have reevaluated the biological significance of these and two other phosphosites (S212 and T727). Other than these, we included the hyperactive mutant (*Scant*), thrombocytopenia-associated SNP variant (*FLJ*) and three different NCMR deletions (Δ194-725, Δ305-620, and Δ385-523) of Mastl in the study. We obtained viable Mastl knockout mouse embryonic fibroblast clones that express the ectopic *FLJ*, *Scant*, S861A, or S861D mutants or the ectopic wild type form of mouse Mastl. Given the vital role of turn motif phosphosite (S861 in mouse) in AGC kinase activation, we focused our research on the functional characterization of this phosphosite.

2. METHODS

2.1. The web servers and programs

The visualized crystal structures were obtained from the Protein Data Bank (PDB) (https://www.rcsb.org/) (Berman et al., 2000). The coordinate files were visualized by using PyMOL (version 2.4.0a0) (Schrödinger, LLC, 2015). By using the sequence alignments given in one of the reference studies (Blake-Hodek et al., 2012), the domain and motif boundaries were determined by using the Uniprot database (https://www.uniprot.org/) (The UniProt Consortium, 2019) and EMBOSS Needle webserver (https://www.ebi.ac.uk/Tools/psa/emboss_needle/) (Rice et al., 2000). Briefly, the FASTA format sequences were obtained from Uniprot and the pairwise sequence alignments were performed using EMBOSS Needle. Based on the determined motif boundaries, the motifs were annotated on the 3D structure visuals when necessary.

CLC Main Workbench 7.9.1 software was used for sequence visualization and processing (https://digitalinsights.qiagen.com). The gel images, immunoblot images, and micrographs were processed using Adobe Photoshop CS6, Adobe Photoshop CC 2019 (Adobe Inc., 2019), and GIMP (version 2.10.12) (The GIMP Development Team, 2019).

2.2. Molecular cloning

The pFastBAC HT B-HA-Mastl WT (KDB53), pBABE-puro (KDB73), pBABE-puro HA-Mastl KD (KDB47), pBABE-puro HA-Mastl FLJ (KDB78), and pBABE-puro HA-Mastl *Scant* (KDB48) expression vectors were obtained from Kaldis laboratory (Institute for Molecular and Cell Biology, Agency for Science, Technology and Research, Singapore, Republic of Singapore). The mutant Mastl cDNAs used in this study were obtained by site-directed mutagenesis. The wild type Mastl cDNA was mutated and subcloned from pFastBAC HT B-HA-Mastl WT vector (KDB53) into the empty pBABE-puro retroviral expression vector (KDB73). The primers used for cloning, site-directed mutagenesis, colony PCR, and Sanger sequencing were given in Table S1. The Mastl variant cDNAs were produced using Q5 high-fidelity DNA polymerase (M0491S; NEB). The restriction cloning of the cDNAs were carried out using Fast Digest BstXI (ER1021; Thermo Scientific), Fast Alkaline Phosphatase (EF0654; Thermo Scientific), and T4 DNA ligase (EL0011; Thermo Scientific), respectively.

2.3. PCR genotyping

A three primer system was utilized for genotyping of Mastl wild type, FLOX, and NULL alleles. The primers used for genotyping; Primer_1 (KDO198), _2 (KDO227), and _3 (KDO228) were given in Table S1. The genotyping strategy for the mouse Mastl loci is depicted in Figure S2. For the PCR genotyping, the samples were prepared according to the adapted HotSHOT protocol (Truett et al., 2000). Briefly, the PBS-washed cell clumps were suspended in an alkaline lysis reagent (25 mM NaOH, 0.2 mM disodium EDTA). The suspension is thoroughly vortexed. Using a thermal block, the samples were boiled for 20-30 minutes under rigorous shaking to extract the genomic DNA. After that, the samples were cooled on ice for approximately 5 minutes. An equal volume of neutralizing reagent (40 mM Tris-HCl) was added to each sample and the samples were vortexed before each use. The genomic DNA samples were stored at -20°C until use. For the genotyping PCR, 1 to 7 µL of DNA sample and 0.625 units of Taq DNA polymerase (A111103; Ampliqon) was used for each 25 µL of reaction volume. 34-40 PCR cycles with 30 seconds denaturation at 94°C, 30 seconds annealing at 67°C, and 30 seconds extension at 72°C were performed. 3 minutes initial denaturation 94°C and 2 minutes final extension at 72°C were performed. The resulting genotyping PCR products were 304bp or 500 bp for Mastl^{dFLOX} or Mastl^{NULL} alleles, respectively.

2.4. Cell culture

The PLAT-E and Mastl conditional knockout MEFs were grown in high-glucose DMEM (D5671-6X500ML; Sigma) or DMEM/F12 (31330038; Gibco) supplemented with 10% FBS (10270106; Gibco), and 1% penicillin/streptomycin (P4333; Sigma). Cells were cultured in a 95% humidified incubator with 5% CO_2 at 37°C. For maintenance, the cells were passaged upon reaching 70-100% confluence.

2.4.1. Transfection and retrovirus packaging

PLAT-E cells were grown under selective pressure with 2-4 µg/ml puromycin and 5-10 µg/ml blasticidin. The selection antibiotics were omitted during and after transfection for ecotropic retrovirus packaging. PLAT-E cells were transfected at 90% confluence in the absence of selective pressure. Transfection with the pBABE puro HA-Mastl DNA constructs was carried out using Lipofectamine 3000 transfection reagent (L3000015; Thermo Scientific), according to the manufacturer's instructions.

The transfection and virus production were carried out in 12-well plate format. For each transfection, the viral supernatant was harvested 48 hours and 72 hours post-transfection. The cell debris was removed by centrifugation at 300xg for 5 minutes. The clarified viral media were stored in new sterile tubes at 4°C up to a week until use.

2.4.2. Transduction and stable cell line engineering

Polybrene was added to a final concentration of 8 µg/mL and mixed, immediately before infection. MEFs were transduced at 40% confluence. Viral media collected at the second day of transfection was used in the first round of transduction. 24h post-transduction, the used viral media was removed and a second round of transduction was performed using the remaining batch of viral media. 8 hours after the second round of transduction, the used viral media was removed. The cells were cultured in normal growth medium overnight for recovery, prior to antibiotic selection. Pool stable cell lines were generated under 2-4 µg/mL puromycin selection. Cells were selected for a week and negative control cells died within the first 2 days of selection. Knockout was induced by adding 20 ng/mL 4-OHT to the culture medium. The control cells were treated with an equal volume of DMSO. The knockout induced stable cell lines were subjected to limited dilution 6 days post-induction.

2.4.3. Mitotic arrest of MEFs

In order to analyze the hyperphosphorylation states of the Mastl variants, the mitotic cells were enriched by 500 ng/mL nocodazole treatment. The nocodazole treatment was initiated when the cells were actively dividing, during the log phase of growth. For protein analysis, the cells were harvested after 2, 4, or 8 hours of nocodazole treatment.

2.5. Western blot and immunocytochemistry

Commercially available primary antibodies used for immunoblot staining are rat anti-HA tag (clone 3F10, 11867423001; Roche) and mouse anti-HSP90 (610419; BD Transduction Laboratories) monoclonal antibodies. The secondary antibodies used for immunoblot staining are HRP-linked goat anti-rat IgG (7077P2; Cell Signaling Technology), HRP-linked goat anti-rabbit IgG (7074P2; Cell Signaling Technology), and HRP-linked goat anti-mouse IgG (7076P2; Cell Signaling Technology) antibodies. Alexa Fluor 488 goat anti-rabbit secondary antibody (4412) was purchased from Cell

Signaling Technology and used for immunocytochemistry. The rabbit anti-Mastl polyclonal primary antibody had been produced in Kaldis laboratory (Institute for Molecular and Cell Biology, Agency for Science, Technology and Research, Singapore, Republic of Singapore) (Diril et al., 2016) and was used for immunoblot and immunocytochemistry staining. Every antibody mentioned herein, except for Alexa Fluor 488 goat anti-rabbit secondary antibody, were kindly provided by Philipp Kaldis (Institute for Molecular and Cell Biology, Agency for Science, Technology and Research, Singapore, Republic of Singapore).

2.6. Cell viability and proliferation assays

The alamarBlue proliferation assay was carried out in 96-well plate format in three replicates. The daily measurements were initiated 24 hours post-seeding. For each day, the cells were incubated in 150 µL of assay medium for approximately 4 hours. The assay medium was prepared by diluting 1 volume of alamarBlue dye reagent (BUF012A; Bio-Rad) in 9 volumes of growth medium. The metabolic activity was quantified fluorometrically by exciting the samples at 560 nm and recording the emission at 590 nm. The assay was performed for 6 successive days.

The proliferation rate in terms of cell division was measured by hemocytometer cell counting. The method is modified from 3T3 assay (Diril et al., 2012). The cell counting assay was carried in 6-well plate format. The assay was initiated by seeding 20,000 cells/well. Every 3 days, the cells were trypsinized and counted. 20,000 cells were reseeded per well. The assay was performed for 4 successive passages.

3. RESULTS

3.1. A robust rescue-assay for coarse phenotypic characterization of the Mastl mutants

A workflow was designed in order to assess the biological significance of the previously described mutations. Briefly, we first ectopically expressed the Mastl variants, then induced knockout, and characterized the phenotype. Due to the depletion of endogenous Mastl, the observed phenotype could be attributed to the ectopic products. The phosphosites of interest are T193, T206, S212, T727, and S861. For the phosphosite studies, we have used the T193V, T206V, S212A, T727V, S861A non-phosphorylatable mutants and the T193E, T206E, S861D phosphomimetic mutants. Other Mastl variants in the present study are *FLJ* and *Scant* point mutations and Mastl(Δ194-725), Mastl(Δ305-620), Mastl(Δ385-523) NCMR deletions. From here on, each cell line will be referred with its given corresponding mutation or deletion remarks. The uninduced parental cell line and the ectopic kinase dead or wild type Mastl expressing cell lines will be referred as ‘parental’, ‘WT’, and ‘KD’ cell lines, respectively.

Upon generation of the stable cell lines, we induced knockout and monitored the cell growth at days 0, 3, and 14. Each cell population was sampled for PCR genotyping at days 3 and 14 to monitor the changes in the proportion of successfully induced cells and cells that had escaped knockout. Due to the nature of inducible Cre systems, each cell line has a basal level of knockout cells as a result of spontaneous Cre leakage into the nucleus, in this case even without 4-OHT induction (Hans et al., 2011; Zhong et al., 2015). Three days post-induction, practically complete knockout was observed for each cell population. However, within fourteen days, initially undetectable numbers of uninduced cells (both homozygous and heterozygous) have proliferated. These uninduced cells became significant or dominant for each cell line, except for the ectopic WT HA-Mastl expressing cell line (Figure 5). Cells escaping knockout is a known disadvantage of the inducible Cre systems (Bao et al., 2013; Song & Palmiter, 2018).

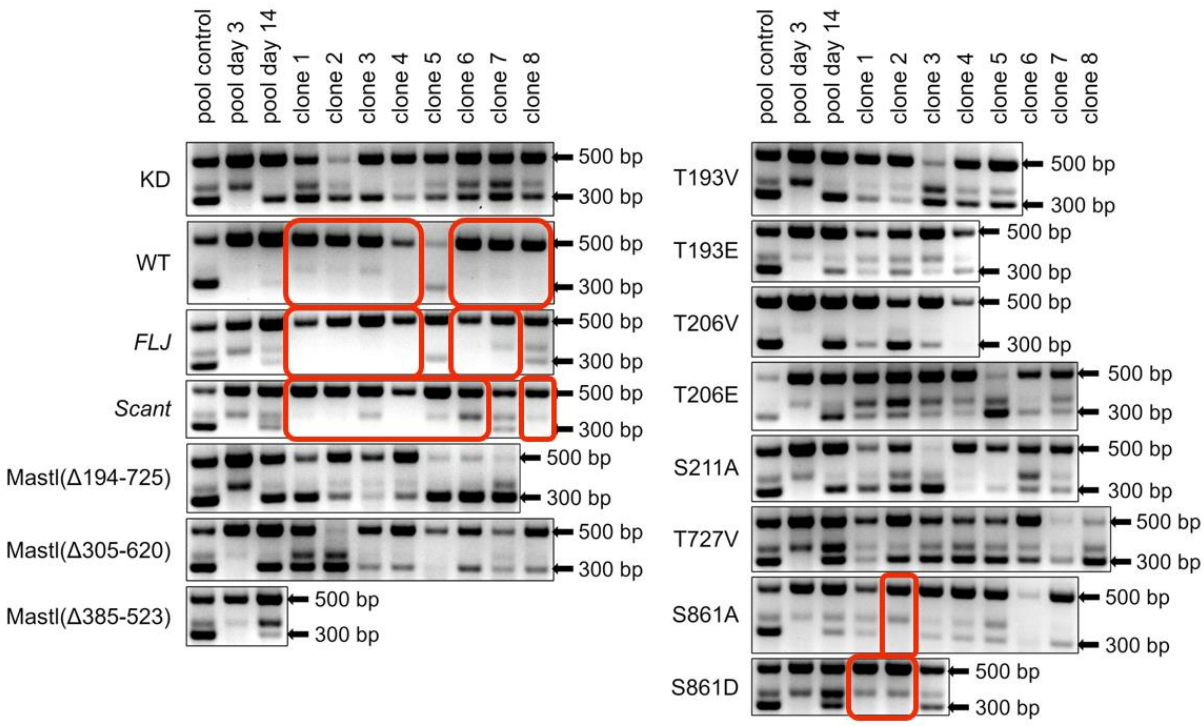

Figure 5. The conditional knockout MEFs were transduced and selected by using their puromycin resistance. Knockout was induced by 20 ng/mL 4-OHT treatment. The stable cell lines were genotyped before induction, 3-days post-induction, and 14 days post-induction. During the experiments, the cells were split six days post-induction and the passage remains were used for single cloning. After colonies had formed, for each cell line, at most eight clones were expanded and genotyped. The 300 and 500 bp bands indicate the presence of double floxed and recombined (knockout) DNA, respectively. The knockout clones were indicated with red round rectangles.

Considering these facts and the essentiality of Mastl for proliferation, we decided to use this technical obstacle of knockout escapers to our advantage. We monitored the genotype of the cell pools as a means to determine whether the mutant Mastl variants can rescue the loss of function phenotype. Briefly, using the ectopic KD Mastl expressing induced cell line as a negative control, and ectopic WT Mastl expressing induced cell line as a positive control, we could infer to what degree the Mastl variants could rescue the knockout phenotype. Even after fourteen days of culturing, trace amounts of uninduced cells had emerged in the ectopic WT Mastl expressing population. On the other hand, ectopic KD Mastl expressing population shows a distinct heterozygous knockout genotype (Figure 5). These results verified the notion that ectopic WT Mastl expression rescued Mastl knockout, therefore knockout

escapers could not take over the population. Furthermore, single clones were isolated from each induced cell line and genotyped. For each cell line, at most a total of eight clones were genotyped when possible (Figure 5). All of the clones derived from the KD cell line were uninduced. Seven out of eight clones derived from the WT HA-Mastl expressing cell line were homozygous knockout. These results together show that our experimental approach works from a proof of principle perspective.

It is known that the Mastl deficient cells cannot proliferate, as a result, Mastl-null cells show significant visual phenotypes such as enlarged cell size and multilobular nuclei. This is an advantage in terms of ease of analysis, because such abnormalities can be detected without requiring delicate techniques. Proliferation rate and morphological features of the knockout induced and control group cell lines were initially analyzed by bright field microscopy (Figure 6).

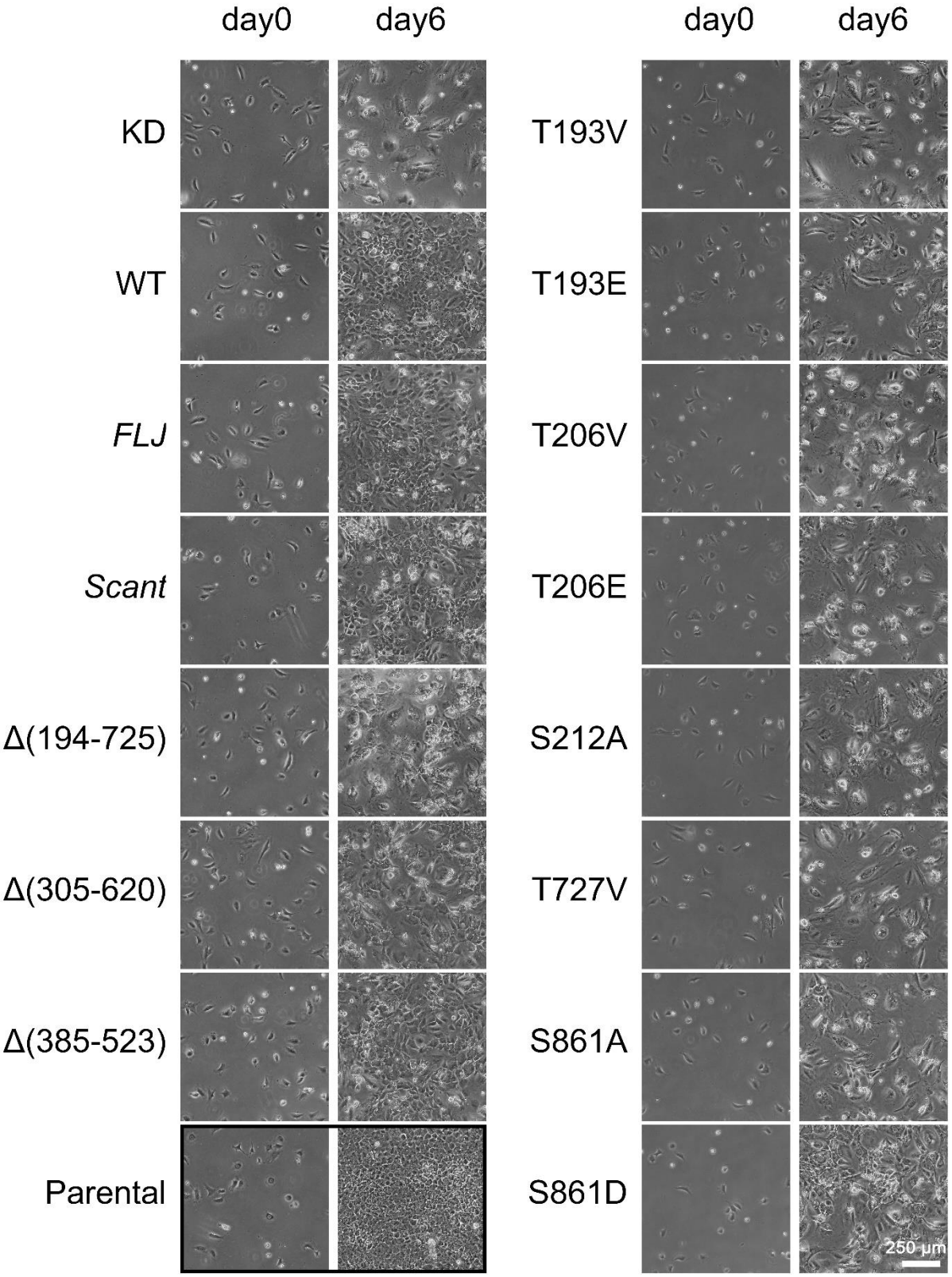

Figure 6. Bright field micrographs of the knockout induced stable cell lines. Knockout was induced by 20 ng/mL 4-OHT treatment. The images were acquired at the day of induction (day 0) and 6 days post-induction. Scale bar is 250 µm.

Stable cells were seeded at low density and similar amounts before induction. At day six, it is visible that the ectopic WT Mastl could rescue the loss of endogenous Mastl the most. *Scant* and *FLJ* variants could also rescue the knockout phenotype, but with visibly less efficiently. On the other hand, we cannot rule out the fact that this may be a result of inequal ectopic expression levels. It is also possible that for each cell line, the ectopic expression levels may not be sufficient. Because we have repeatedly observed that DMSO treated parental cell line proliferated at a visibly faster rate than 4-OHT treated ectopic WT Mastl expressing cell line.

Cell lines which failed to rescue the loss of endogenous Mastl have undergone senescence as observed in the micrographs taken at day six. Cells were analyzed periodically until day fourteen and we observed that the proportion of morphologically abnormal cells decreased and morphologically normal cells gradually dominated the population (data not shown), consistent with the cell pool genotyping results.

3.2. The turn motif phosphosite deficient Mastl is viable

Our initial clone screening shows that we have captured three turn motif phosphosite mutant clones that are homozygous knockout. One of them is unphosphorylatable (S861A) and the other two are the phosphomimetic (S861D) mutants (Figure 5). As thoroughly explained, the role of turn motif phosphorylation is known to be crucial for AGC kinase activation. Therefore, we focused our research on these knockout clones for functional characterization of this particular phosphosite.

Protein analysis of the clones shows that the ectopic Mastl in the S861A mutant is a partially unknown fusion product (Figure 7). In this regard, we suspect that during the genomic integration, the exogenous Mastl DNA might have been integrated in a highly expressed endogenous open reading frame. Mastl has a unique electrophoretic mobility. Despite Mastl is a ~120 kDa protein, it migrates alongside with the 100 kDa molecular weight marker (data not shown). Given that, it is possible that 195 kDa can be an underestimated molecular weight of this fusion product.

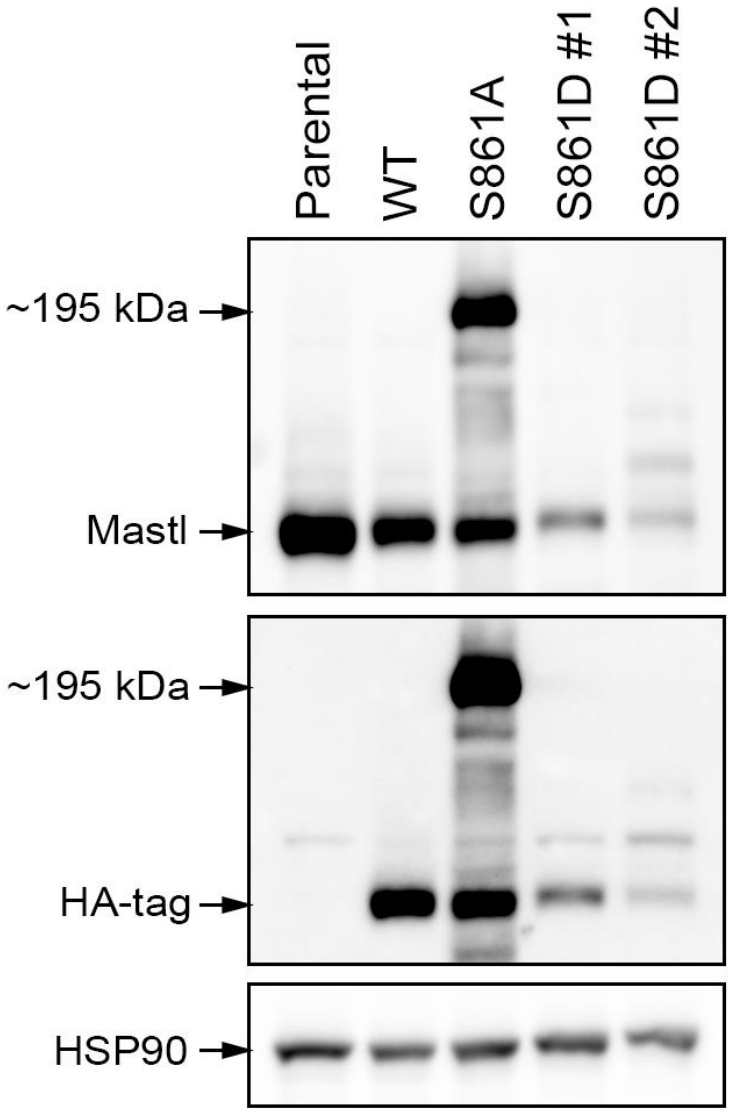

Figure 7. Western blot analysis of Mastl expression in the chosen clones. Total and ectopic (HA-tagged) Mastl levels of the parental cell line (control), a knockout WT clone (control), and the knockout phosphosite clones are given. HSP90 was used as the loading control. The upper, middle, and lower panels are Mastl, HA tag, and HSP90 immunoblots, respectively.

The parental cell line shows the highest total Mastl expression. The expression level of the fused Mastl S861A product is comparable to the endogenous Mastl level of the parental cell line. The expression of the fused Mastl S861A product dominates

the normal Mastl S861A product. The western blot analysis is consistent with the immunocytochemical analysis of total Mastl expression (Figure 8).

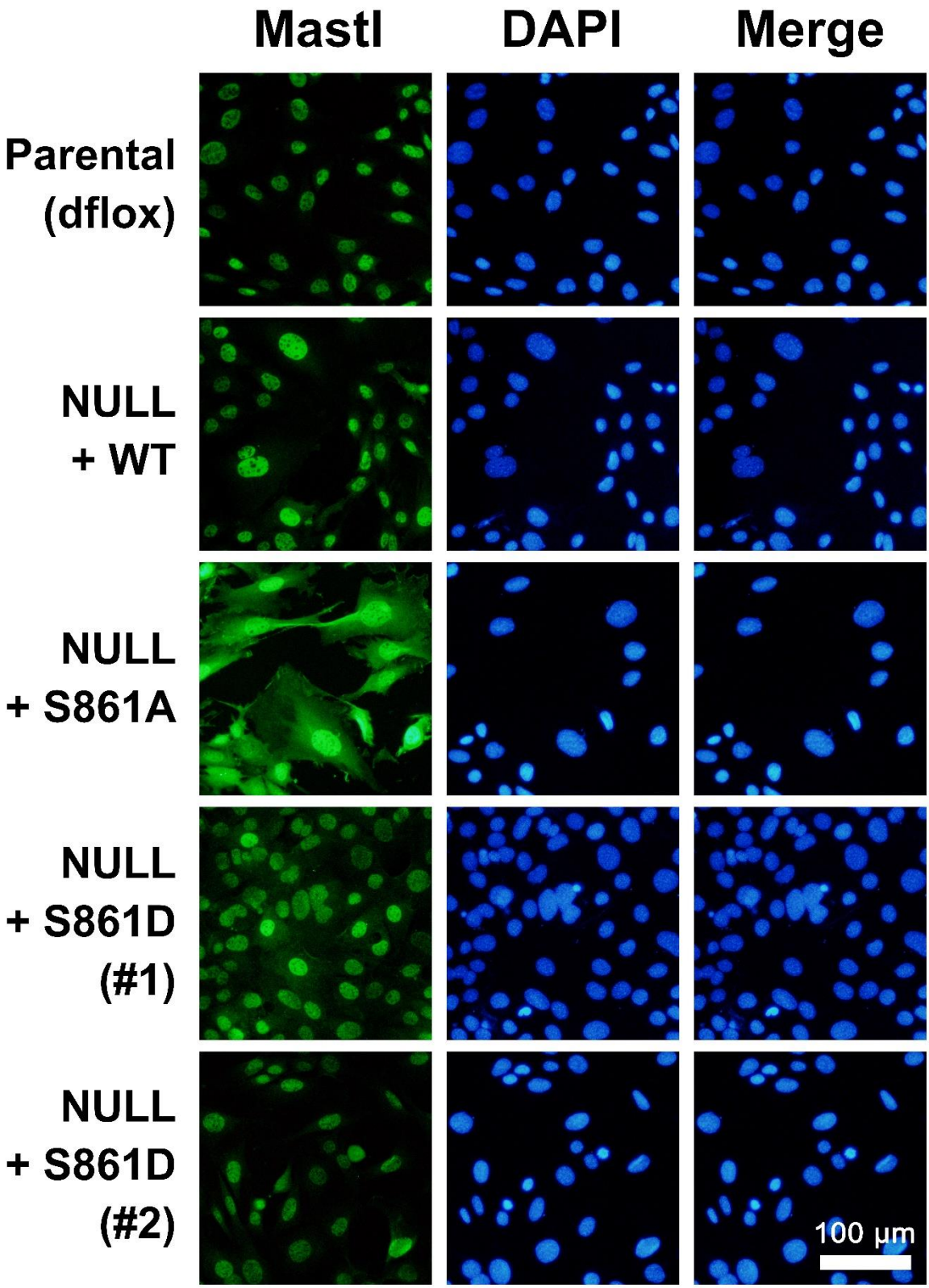

Figure 8. The total Mastl expression in the chosen clones were analyzed by immunocytochemistry. Total Mastl content (green) and the nuclei were stained (blue). Scale bar is 100 µm.

Mastl is located in the nucleus during interphase (Yu et al., 2004). In the immunocytochemistry analysis, it is observed that Mastl leaks to cytoplasm in interphasic cells. However, this occurrence is attributed to the presence of the fused Mastl S861A product. It is possible that this product is unstable, thus leading to formation of the degradation products. We hypothesized that the degradation products may encompass the consensus sequence that the anti-Mastl antibody recognizes. As a result, the degradation products can be stained. This explains the lower molecular weight smears in the Western blot (Figure 7), and the cytoplasmic Mastl staining in immunocytochemistry. The leakage of the possible degradation products can be explained by the fact that they lose the motifs and interaction sites that keeps the intact Mastl in nucleus during interphase. Nevertheless, when the protein expression levels of the clones and parental cell line are compared, it is possible that S861A clone compensates for the of enzyme activity with high Mastl expression.

3.3. The Mastl S861 phosphosite mutants and the wild type Mastl display different phenotypes

The proliferation rate of parental cell line and WT, S861A, and S861D clones were compared by different means. The absolute proliferation rate of the cell lines was compared by cell counting as a measure of the cell division rates. The proliferation rate in terms of metabolic activity was measured using alamarBlue proliferation assay. Based on the metabolic activity, intriguingly, the proliferation rate of each cell line is comparable (Figure 9A). Based on their cell division rates, it is observed that the phosphosite mutants proliferate several folds slower when compared to the ectopic WT Mastl expressing knockout clone and the parental cell line (Figure 9B).

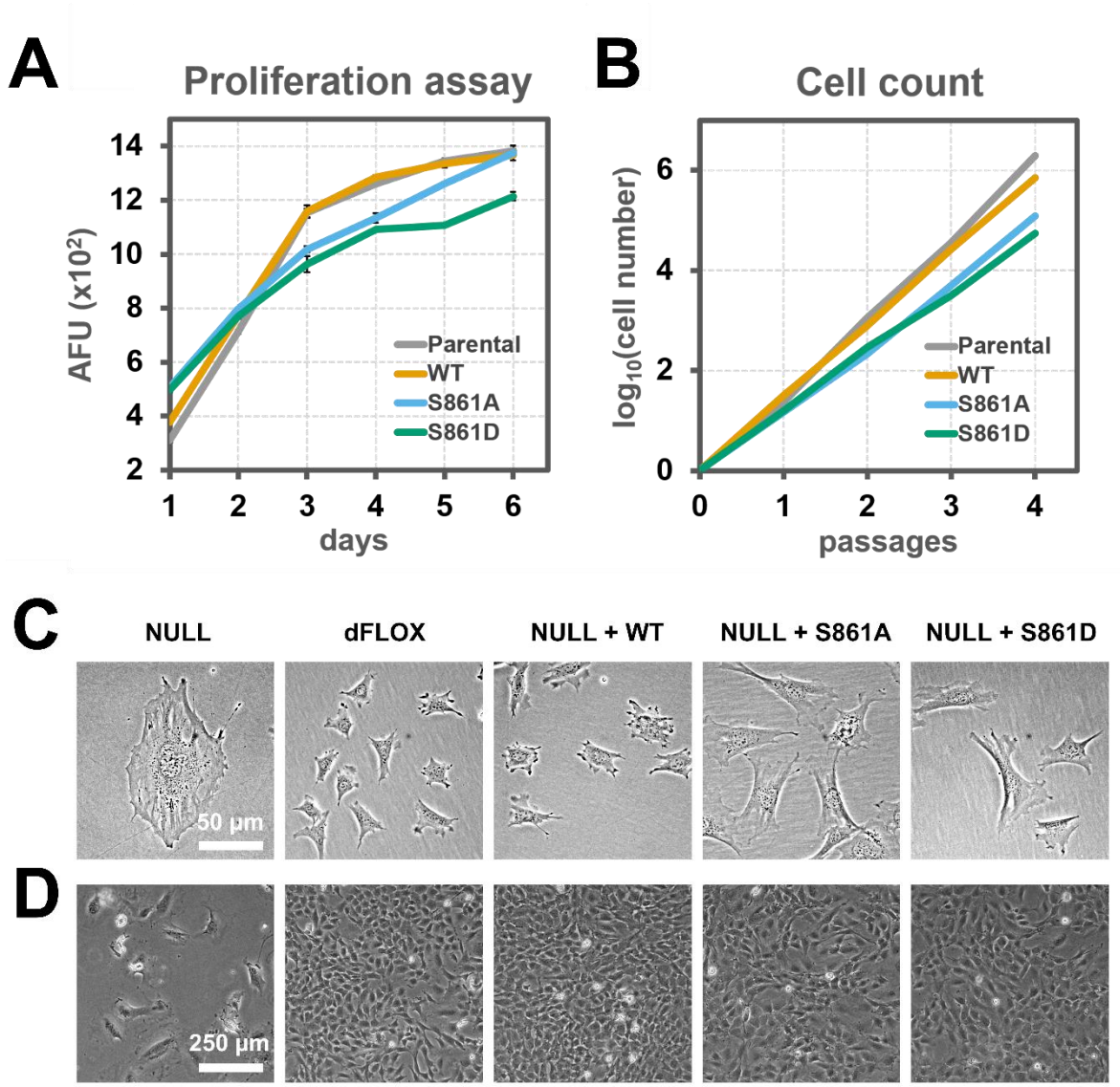

Figure 9. Proliferation rates and morphologies of the parental cell line and WT, S861A, or S861D mutant Mastl expressing knockout single clones. (A) alamarBlue proliferation assay of the given cell line and clones. The metabolic activity of the cell lines was fluorometrically measured in terms of the resazurin reduction capacity. The cells were monitored for six days. (B) The cell counts of the given cell line and clones. The proliferation rate in terms of cell division was measured by hemocytometer cell counting. The cell amounts were monitored for four passages. (C) The cells were seeded at low density in order to show their unique morphologies in the absence of cell-cell contact restrictions. Scale bar is 50 µm. (D) In a 6-well plate, the semi-confluent asynchronous cells were treated with DMSO or 20 ng/mL 4-OHT. The next day, 20,000 cells/well were seeded. The bright field images were acquired three days later. Scale bar is 250 µm.

It is possible that the phosphosite mutant forms of Mastl are partially active so that it can satisfy its mitotic tasks to a degree. As a result, the cell cycle can be completed, but the time required for completion of the cell cycle is prolonged. The cell growth and cell division are partially impaired, yielding morphologically unique and larger cells with overall rare occurrence of multilobular nuclei in the population. In the alamarBlue proliferation assay, the assay was initiated with equal amounts of cell for each group. The phosphosite mutants show higher resazurin reduction capacity for approximately the first two days of incubation (Figure 9A). This result is attributed to the larger cell volumes (Figure 9C). The large cells divide slower (Figure 9B) and due to the higher amounts of intracellular content, they are more capable of resazurin reduction. In prolonged incubation, small cells compensate for this reduction activity as their cell cycle is completed in a shorter period of time. For this reason, it takes approximately two days for the parental cell line and the WT clone to reach a resazurin reduction capacity that is comparable to that of the S861A and S861D clones.

Together, these results suggest that the phosphosite mutants are displaying a mild Mastl knockout phenotype, that is not fatal for the cell cycle unlike the actual Mastl knockout phenotype. It is possible that the phosphosite mutants might have entered a partially senescent state. On the other hand, we observed that the clones are stable in terms of viability. This means that the spontaneous cell deaths and presence of cells with multilobular nuclei are rare. These occurrences are comparable among each cell group, except for the 4-OHT-treated parental cell line, which displays the true Mastl knockout phenotype. In this regard, it should be noted that the fact that S861A and S861D clones are proliferating slowly, does not mean that the clones are sick. In fact, the difference of the proliferation rate is not dramatic that it requires monitoring for several passages by cell counting to capture a distinct difference (Figure 9B). Consistently, the visual examinations show that when equal amounts of cells are seeded at low density, the time required for each cell group to become confluent is similar (Figure 9D). The second S861D clone was excluded from the proliferation assays as its proliferation rate was abnormally low (data not shown), which is consistent with its Mastl expression level (Figure 7). It is evident that the other phosphosite mutant clones (S861A and S861D #2) are viable, they complete their cell cycle in a reasonable period of time.

3.4. Mammalian Mastl kinase is regulated by cis-autophosphorylation

The phenomenon of cis-autophosphorylation has been repeatedly verified on Xenopus Mastl. Blake-Hodek et al. have demonstrated that active wild type Mastl purified from okadaic acid treated Sf9 cells was capable of becoming radiolabeled, whereas kinase dead Mastl was not. This proves the regulation by autophosphorylation. When wild type active Mastl was added to an excess of inactive Mastl, trace amounts of trans-autophosphorylation of the inactive Mastl was observable. Cis-autophosphorylation of the active wild type Mastl was by far the dominant. This proves that the autophosphorylation event is dominated by cis-autophosphorylation. In the present study, we have validated the cis-autophosphorylation model on mouse Mastl using intact MEFs (mouse embryonic fibroblasts). In parallel experiments, we ectopically expressed the wild type or kinase dead HA-tagged mouse Mastl in uninduced MEFs. To perform the protein analysis on the active state of Mastl, the cells were treated with nocodazole for different time intervals to enrich the mitotic cells. The prolonged nocodazole treatment is accompanied by an accumulation of the phosphorylated mitotic proteins. Proportion of the phosphorylated Mastl increases. The hyperphosphorylated Mastl has a decreased electrophoretic mobility, which is observed as a band upshift in the immunoblots. The HA tag blots of this experiment show that the MEFs expressing wild type HA-Mastl are capable of this upshift. Whereas an electrophoretic mobility change could not be observed in case of the kinase dead (KD) HA-Mastl expressing MEFs (Figure 10A). When the results are evaluated together, it is clear that the endogenous wild type Mastl cannot significantly phosphorylate the KD HA-Mastl. Therefore, the band upshift of the WT HA-Mastl is attributed to cis-autophosphorylation. Unlike the results obtained by Blake-Hodek et al., we could not observe a trace amount of trans-autophosphorylation. A possible explanation for this can be that the different protein detection techniques may have different limits of detection.

3.5. The turn motif phosphosite deficient Mastl is capable of cis-autophosphorylation

Our initial analyses of the S861A knockout clone show that despite it is viable, it has abnormal features when compared to the control cells. Cell division rate of the S861A/D clones are lower. Using bright field microscopy, examination of the adhered and suspended states of the cell lines has shown that S861A/D clone is larger in size,

both in terms of cell surface area and cell volume (data not shown). These results together show that the S861A/D clones display a mild Mastl knockout phenotype. The observable phenotype together with the function of this phosphosite indicate that the S861A mutation might have impaired the enzyme activity. Expanding on this, we investigated whether Mastl S861A can become hyperphosphorylated. To that end, using the parental cell line, the WT and S861A knockout clones, we followed the same experimental setup that we described under this results section.

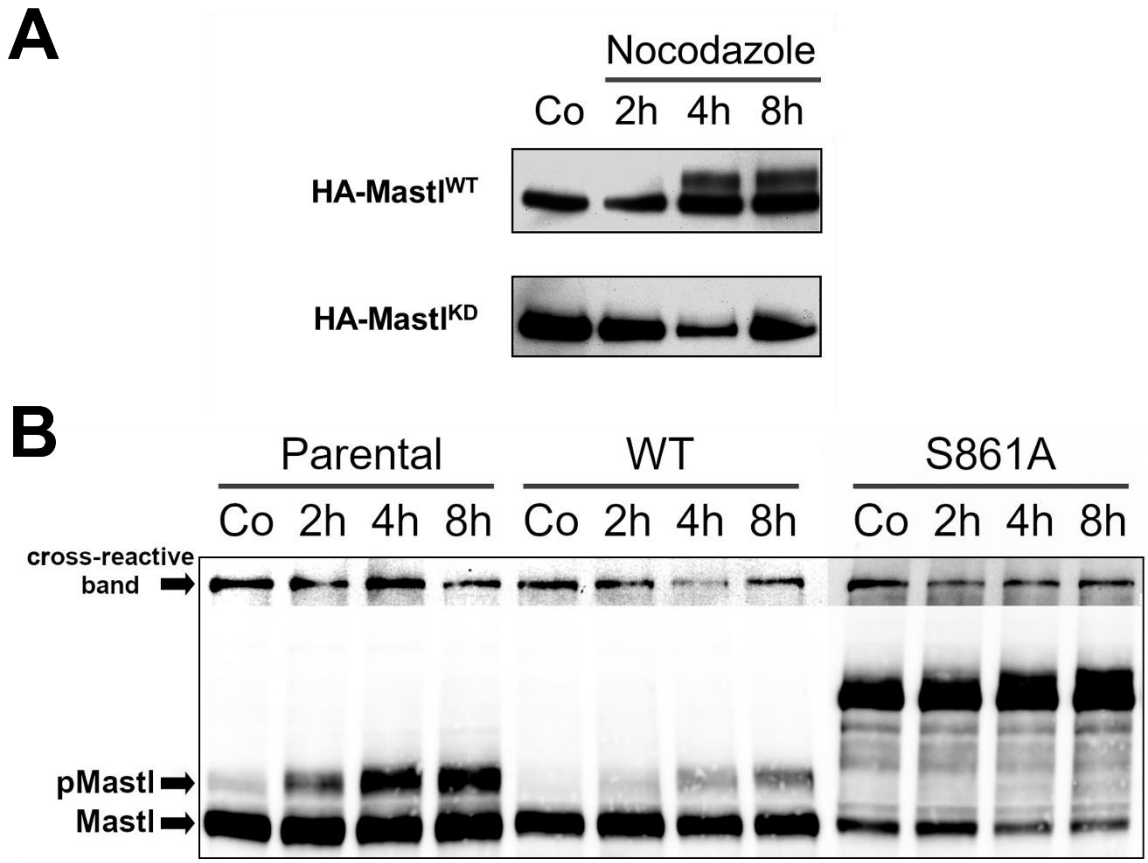

Figure 10. EMSA (electrophoretic mobility shift assay) of mitotic hyperphosphorylation of Mastl. Each cell group was experimented in four subgroups based on the duration of nocodazole exposure. The control subgroups (Co) were not nocodazole treated and the others were nocodazole treated for two, four, or eight hours. (A) HA tag immunoblots of the polyclonal MEFs expressing the wild type or kinase dead HA-Mastl. (B) Mastl immunoblots of the parental cell line, and ectopic WT or S861A mutant Mastl expressing knockout clones. The unidentified high molecular weight cross-reactive band was overexposed post-acquisition in order to be used as the protein loading control.

For the S861A clone, we could not observe an upshift of the normal molecular weight Mastl. However, we observed a slight upshift of the fused Mastl S861A product (Figure 10B). Given the visible molecular weight difference between the normal Mastl and the fused Mastl S861A, it is possible that this slight upshift of the larger Mastl corresponds to a longer upshift of the normal Mastl. On the other hand, a band upshift could not be observed for the normal molecular weight Mastl in S861A clone. It is possible that the degradation products of the larger Mastl mask such weak bands. Based on this, it can be hypothesized that Mastl S861A is capable of cis-autophosphorylation.

4. DISCUSSION

In AGC kinases, the activation loop and C-tail phosphorylations are crucial for kinase activation. Activating phosphorylations govern the conformational transition from inactive to active state through intramolecular allosteric interactions. A feature that makes Mastl a unique AGC kinase, other than its long NCMR domain, is that it has a functional N-lobe hydrophobic pocket, yet it is devoid of a functional HF motif to bind. An example protein kinase that shares this unique feature is PDK1. PDK1 circumvents this structural shortfall by binding the HF motif of other AGC kinases to achieve complete activation (R. M. Biondi, 2001; Ricardo M. Biondi et al., 2000). Expanding on this, Vigneron et al. had demonstrated that a partially active mutant form of Mastl could achieve 156% of its basal activity in the presence of a synthetic peptide (PIFtide) that contains the hydrophobic motif. On the other hand, inactive wild type Mastl could not become active alone. Therefore, Mastl allegedly works as heterodimers, with the HF motif of its partner docked to the hydrophobic pocket on the N-lobe of Mastl. This result of Vigneron et al. is consistent with that of our own (Figure 10A). On the other hand, they had measured the enzyme activity as a means of turn motif phosphorylation. This means that, they have deduced the turn motif phosphorylation as a requirement for intermolecular HF motif docking. However, turn motif-phosphorylated Mastl is not the only active state of Mastl. There is a partially active transition state of the enzyme that occurs with activation loop phosphorylation. This takes place before the turn motif phosphorylation event. Our results suggest that the turn motif phosphorylation is dispensable for the mitotic functions of Mastl.

5. CONCLUSION

When our results and the results of Vigneron et al. are evaluated together, it is clear that the intermolecular HF motif docking require a partially active Mastl. However, this does not strictly involve the turn motif phosphorylation or C-tail docking. About a decade after the initial studies that had characterized the activation mechanism of Mastl (Blake-Hodek et al., 2012; Vigneron et al., 2011), the subject still has an ambiguous aspect to it. An ultimate solution can be offered by structural studies that will aim to probe the determinants of intermolecular HF motif docking. In this regard, a basic system design may ideally involve an ATP and two Mg^{2+} cations coordinated in the ATP binding pocket of an NCMR truncated Mastl. The peptide binding groove should be occupied with an inhibitor peptide. The wild type Mastl construct that will be used for such a study must possess the full-length C-tail domain. Co-crystal structure of the described wild type Mastl and an optimal HF motif peptide can be determined. In parallel, this experiment should be performed on the turn motif unphosphorylatable or phosphomimetic mutants of Mastl. Supporting the structural interpretations with binding kinetics or enzyme kinetics data is crucial. In this case, binding affinity of the given Mastl variants to the HF motif should be measured rather than measuring the kinase activity. Alternatively, the kinase activity of the Mastl variants can be measured in the presence of the HF motif peptide. However, the latter method would be an indirect measure of HF motif binding. Therefore, the former method is more reliable. In case of the experimental approach, active Mastl should be used as the starting material. For that purpose, okadaic acid treated Sf9 cells are used in general. In case of the computational approach, the above-mentioned systems can be obtained by homology modeling, followed by docking. The C-tail and HF motif peptide conformations can be optimized by molecular dynamics simulations, followed by the energetic analysis of the systems. In this way, it can be understood whether the free energy contributions of the turn motif phosphate to HF motif docking are significant.

Our results contribute to the currently accepted model for Mastl kinase activation. In possible future studies, the above-mentioned structure-based workflows hopefully resolve the remaining uncertainties and conflicts regarding the Mastl activation. It should be kept in mind that resolving the mysteries of Mastl activation may aid other similar researches that target such unique AGC kinases.

ASSOCIATED CONTENT

Supporting Information

Supporting tables and figures that are mentioned in the text are given.

AUTHOR INFORMATION

Corresponding Author

*E-mail: kasim.diril@ibg.edu.tr

Author Contributions

The manuscript was written through contributions of all authors. All authors have given approval to the final version of the manuscript.

ORCID

Mehmet Erguven: 0000-0001-5947-8568

M. Kasim Diril: 0000-0002-3644-4178

Notes

The authors declare no competing financial interest.

ACKNOWLEDGEMENTS

We thank Dr. Philipp Kaldis and his team for sharing the vectors, bacterial glycerol stocks, and antibodies that were used in this study. We thank Dr. Esra Erdal, Dr. Gunes Ozhan, Dr. Mehmet Ozturk, Dr. Nese Atabey, Dr. Serif Senturk, Dr. Sermin Genc, Dr. Yavuz Oktay, and their teams for sharing their research consumables or instruments with us.

This work was supported by Dokuz Eylul University Scientific Research Projects grant (DEU-BAP Project No: 2016.KB.SAG.014). Kasim Diril received additional support from Turkish Academy of Sciences (GEBIP award) and The Science Academy, Turkey (BAGEP award). Mehmet Erguven was supported by a stipend from TUBITAK (The Scientific and Technological Research Council of Turkey) Project No. 217Z248.

ABBREVIATIONS

4-OHT, 4-Hydroxytamoxifen; DMSO; dimethyl sulfoxide; HA, Human influenza hemagglutinin; HF, Hydrophobic Motif; MEF, Mouse Embryonic Fibroblast; MUT,

Mutant; NCMR, Non-Conserved Middle Region; NLT, N-Lobe Tether; PDB, The Protein Data Bank; SAC, Spindle Assembly Checkpoint; WT, Wild Type.

REFERENCES

Adams, J. A. (2003). Activation Loop Phosphorylation and Catalysis in Protein Kinases: Is There Functional Evidence for the Autoinhibitor Model? *Biochemistry*, *42*(3), 601–607. https://doi.org/10.1021/bi020617o

Adobe Inc. (2019). *Adobe Photoshop* (CC 2019) [Computer software]. https://www.adobe.com/products/photoshop.html

Alberts, B. (2015). *Ch 17: Cell Cycle*. https://doi.org/10.1017/CBO9781107415324.004

Alvarez-Fernandez, M., Sanchez-Martinez, R., Sanz-Castillo, B., Gan, P. P., Sanz-Flores, M., Trakala, M., Ruiz-Torres, M., Lorca, T., Castro, A., & Malumbres, M. (2013). Greatwall is essential to prevent mitotic collapse after nuclear envelope breakdown in mammals. *Proceedings of the National Academy of Sciences*, *110*(43), 17374–17379. https://doi.org/10.1073/pnas.1310745110

Bao, J., Ma, H. Y., Schuster, A., Lin, Y. M., & Yan, W. (2013). Incomplete cre-mediated excision leads to phenotypic differences between Stra8-iCre; Mov10l1lox/lox and Stra8-iCre; Mov10l1lox/Δ mice. *Genesis*, *51*(7), 481–490. https://doi.org/10.1002/dvg.22389

Baxter, R., Hastings, N., Law, a., & Glass, E. J. . (2008). Harvey Lodish, Arnold Berk, Chris A. Kaiser, Monty Krieger, Anthony Bretscher, Hidde Ploegh, Angelika Amon, Kelsey C. Martin-Molecular Cell Biology-W. H. Freeman (2016). In *Animal Genetics*. https://doi.org/10.1017/CBO9781107415324.004

Berman, H. M., Westbrook, J., Feng, Z., Gilliland, G., Bhat, T. N., Weissig, H., Shindyalov, I. N., & Bourne, P. E. (2000). The Protein Data Bank. *Nucleic Acids Research*, *28*(1), 235–242. https://doi.org/10.1093/nar/28.1.235

Biondi, R. M. (2001). The PIF-binding pocket in PDK1 is essential for activation of S6K and SGK, but not PKB. *The EMBO Journal*, *20*(16), 4380–4390. https://doi.org/10.1093/emboj/20.16.4380

Biondi, Ricardo M., Cheung, P. C. F., Casamayor, A., Deak, M., Currie, R. A., & Alessi, D. R. (2000). Identification of a pocket in the PDK1 kinase domain that interacts with PIF and the C-terminal residues of PKA. *The EMBO Journal*, *19*(5), 979–988. https://doi.org/10.1093/emboj/19.5.979

Blake-Hodek, K. A., Williams, B. C., Zhao, Y., Castilho, P. V., Chen, W., Mao, Y., Yamamoto, T. M., & Goldberg, M. L. (2012). Determinants for Activation of the Atypical AGC Kinase Greatwall during M Phase Entry. *Molecular and Cellular Biology*, *32*(8), 1337–1353. https://doi.org/10.1128/MCB.06525-11

Ciliberto, A., & Shah, J. V. (2009). A quantitative systems view of the spindle assembly checkpoint. *EMBO Journal*, *28*(15), 2162–2173. https://doi.org/10.1038/emboj.2009.186

Das, A., Gerlits, O., Parks, J. M., Langan, P., Kovalevsky, A., & Heller, W. T. (2015). Protein Kinase A Catalytic Subunit Primed for Action: Time-Lapse Crystallography of Michaelis Complex Formation. *Structure*, *23*(12), 2331–2340. https://doi.org/10.1016/j.str.2015.10.005

Diamant, S., Azem, A., Weiss, C., & Goloubinoff, P. (1995). Effect of Free and ATP-bound Magnesium and Manganese Ions on the ATPase Activity of Chaperonin GroEL14. *Biochemistry*, *34*(1), 273–277. https://doi.org/10.1021/bi00001a033

Diril, M. K., Ratnacaram, C. K., Padmakumar, V. C., Du, T., Wasser, M., Coppola, V., Tessarollo, L., & Kaldis, P. (2012). Cyclin-dependent kinase 1 (Cdk1) is essential for cell division and suppression of DNA re-replication but not for

liver regeneration. *Proceedings of the National Academy of Sciences*, *109*(10), 3826–3831. https://doi.org/10.1073/pnas.1115201109

Diril, M. Kasim, Bisteau, X., Kitagawa, M., Caldez, M. J., Wee, S., Gunaratne, J., Lee, S. H., & Kaldis, P. (2016). Loss of the Greatwall Kinase Weakens the Spindle Assembly Checkpoint. *PLOS Genetics*, *12*(9), e1006310. https://doi.org/10.1371/journal.pgen.1006310

Endicott, J. A., Noble, M. E. M., & Johnson, L. N. (2012). The Structural Basis for Control of Eukaryotic Protein Kinases. *Annual Review of Biochemistry*, *81*(1), 587–613. https://doi.org/10.1146/annurev-biochem-052410-090317

Gharbi-Ayachi, A., Labbé, J. C., Burgess, A., Vigneron, S., Strub, J. M., Brioudes, E., Van-Dorsselaer, A., Castro, A., & Lorca, T. (2010). The substrate of Greatwall kinase, Arpp19, controls mitosis by inhibiting protein phosphatase 2A. *Science*, *330*(6011), 1673–1677. https://doi.org/10.1126/science.1197048

Glover, D. M. (2012). The overlooked greatwall: A new perspective on mitotic control. *Open Biology*, *2*(3), 120023. https://doi.org/10.1098/rsob.120023

Hans, S., Freudenreich, D., Geffarth, M., Kaslin, J., Machate, A., & Brand, M. (2011). Generation of a non-leaky heat shock-inducible Cre line for conditional Cre/lox strategies in zebrafish. *Developmental Dynamics*, *240*(1), 108–115. https://doi.org/10.1002/dvdy.22497

Huse, M., & Kuriyan, J. (2002). The Conformational Plasticity of Protein Kinases. *Cell*, *109*(3), 275–282. https://doi.org/10.1016/S0092-8674(02)00741-9

Kannan, N., Haste, N., Taylor, S. S., & Neuwald, A. F. (2007). The hallmark of AGC kinase functional divergence is its C-terminal tail, a cis-acting regulatory module. *Proceedings of the National Academy of Sciences*, *104*(4), 1272–1277. https://doi.org/10.1073/pnas.0610251104

Kim, H., Fernandes, G., & Lee, C. (2016). Protein Phosphatases Involved in Regulating Mitosis: Facts and Hypotheses. *Molecules and Cells*, *39*(9), 654–662. https://doi.org/10.14348/molcells.2016.0214

Kim, M.-Y., Bucciarelli, E., Morton, D. G., Williams, B. C., Blake-Hodek, K., Pellacani, C., Von Stetina, J. R., Hu, X., Somma, M. P., Drummond-Barbosa, D., & Goldberg, M. L. (2012). Bypassing the Greatwall–Endosulfine Pathway: Plasticity of a Pivotal Cell-Cycle Regulatory Module in *Drosophila melanogaster* and *Caenorhabditis elegans*. *Genetics*, *191*(4), 1181–1197. https://doi.org/10.1534/genetics.112.140574

Kishimoto, T. (2015). Entry into mitosis: A solution to the decades-long enigma of MPF. *Chromosoma*, *124*(4), 417–428. https://doi.org/10.1007/s00412-015-0508-y

Mochida, S., Maslen, S. L., Skehel, M., & Hunt, T. (2010). Greatwall Phosphorylates an Inhibitor of Protein Phosphatase 2A That Is Essential for Mitosis. *Science*, *330*(6011), 1670–1673. https://doi.org/10.1126/science.1195689

Mochida, Satoru, & Hunt, T. (2012). Protein phosphatases and their regulation in the control of mitosis. *EMBO Reports*, *13*(3), 197–203. https://doi.org/10.1038/embor.2011.263

Modi, V., & Dunbrack, R. L. (2019). Defining a new nomenclature for the structures of active and inactive kinases. *Proceedings of the National Academy of Sciences*, *116*(14), 6818–6827. https://doi.org/10.1073/pnas.1814279116

Pearce, L. R., Komander, D., & Alessi, D. R. (2010). The nuts and bolts of AGC protein kinases. *Nature Reviews Molecular Cell Biology*, *11*(1), 9–22. https://doi.org/10.1038/nrm2822

Rice, P. (n.d.). *EMBOSS: The European Molecular Biology Open Software Suite*. 2.

Santamaría, D., Barrière, C., Cerqueira, A., Hunt, S., Tardy, C., Newton, K., Cáceres, J. F., Dubus, P., Malumbres, M., & Barbacid, M. (2007). Cdk1 is sufficient to drive the mammalian cell cycle. *Nature*, *448*(7155), 811–815. https://doi.org/10.1038/nature06046

Schrödinger, LLC. (2015). *The PyMOL Molecular Graphics System, Version 1.8*.

Slupe, A. M., Merrill, R. A., & Strack, S. (2011). Determinants for Substrate Specificity of Protein Phosphatase 2A. *Enzyme Research*, *2011*, 1–8. https://doi.org/10.4061/2011/398751

Song, A. J., & Palmiter, R. D. (2018). Detecting and Avoiding Problems When Using the Cre–lox System. *Trends in Genetics*, *34*(5), 333–340. https://doi.org/10.1016/j.tig.2017.12.008

Takimura, T., Kamata, K., Fukasawa, K., Ohsawa, H., Komatani, H., Yoshizumi, T., Takahashi, I., Kotani, H., & Iwasawa, Y. (2010). Structures of the PKC-$ıota$ kinase domain in its ATP-\-bound and apo forms reveal defined structures of residues 533–551 in the C-terminal tail and their roles in ATP binding. *Acta Crystallographica Section D*, *66*(5), 577–583. https://doi.org/10.1107/S0907444910005639

Taylor, S. S., Keshwani, M. M., Steichen, J. M., & Kornev, A. P. (2012). Evolution of the eukaryotic protein kinases as dynamic molecular switches. *Philosophical Transactions of the Royal Society B: Biological Sciences*, *367*(1602), 2517–2528. https://doi.org/10.1098/rstb.2012.0054

The GIMP Development Team. (2019). *GIMP* (2.10.12) [Computer software]. https://www.gimp.org

The UniProt Consortium. (2019). UniProt: A worldwide hub of protein knowledge. *Nucleic Acids Research*, *47*(D1), D506–D515. https://doi.org/10.1093/nar/gky1049

Truett, G. E., Heeger, P., Mynatt, R. L., Truett, A. A., Walker, J. A., & Warman, M. L. (2000). Preparation of PCR-Quality Mouse Genomic DNA with Hot Sodium Hydroxide and Tris (HotSHOT). *BioTechniques*, *29*(1), 52–54. https://doi.org/10.2144/00291bm09

Vigneron, S., Gharbi-Ayachi, A., Raymond, A.-A., Burgess, A., Labbe, J.-C., Labesse, G., Monsarrat, B., Lorca, T., & Castro, A. (2011). Characterization of the Mechanisms Controlling Greatwall Activity. *Molecular and Cellular Biology*, *31*(11), 2262–2275. https://doi.org/10.1128/MCB.00753-10

Vijayan, R. S. K., He, P., Modi, V., Duong-Ly, K. C., Ma, H., Peterson, J. R., Dunbrack, R. L., & Levy, R. M. (2015). Conformational Analysis of the DFG-Out Kinase Motif and Biochemical Profiling of Structurally Validated Type II Inhibitors. *Journal of Medicinal Chemistry*, *58*(1), 466–479. https://doi.org/10.1021/jm501603h

Yu, J., Fleming, S. L., Williams, B., Williams, E. V., Li, Z., Somma, P., Rieder, C. L., & Goldberg, M. L. (2004). Greatwall kinase. *Journal of Cell Biology*, *164*(4), 487–492. https://doi.org/10.1083/jcb.200310059

Yu, J., Zhao, Y., Li, Z., Galas, S., & Goldberg, M. L. (2006). Greatwall Kinase Participates in the Cdc2 Autoregulatory Loop in Xenopus Egg Extracts. *Molecular Cell*, *22*(1), 83–91. https://doi.org/10.1016/j.molcel.2006.02.022

Zheng, J., Trafny, E. A., Knighton, D. R., Xuong, N., Taylor, S. S., Ten Eyck, L. F., & Sowadski, J. M. (1993). 2.2 \AA refined crystal structure of the catalytic subunit of cAMP-dependent protein kinase complexed with MnATP and a

peptide inhibitor. *Acta Crystallographica Section D*, *49*(3), 362–365. https://doi.org/10.1107/S0907444993000423

Zhong, Z. A., Sun, W., Chen, H., Zhang, H., Lay, Y. A. E., Lane, N. E., & Yao, W. (2015). Optimizing tamoxifen-inducible Cre/loxp system to reduce tamoxifen effect on bone turnover in long bones of young mice. *Bone*, *81*, 614–619. https://doi.org/10.1016/j.bone.2015.07.034

Zhou, T., Commodore, L., Huang, W.-S., Wang, Y., Sawyer, T. K., Shakespeare, W. C., Clackson, T., Zhu, X., & Dalgarno, D. C. (2010). Structural Analysis of DFG-in and DFG-out Dual Src-Abl Inhibitors Sharing a Common Vinyl Purine Template. *Chemical Biology & Drug Design*, *75*(1), 18–28. https://doi.org/10.1111/j.1747-0285.2009.00905.x